2023 IEEE/ASME International Conference on Advanced Intelligent Mechatronics (AIM)
June 28-30, 2023. Seattle, Washington, USA

Reduced-Order Nominal Model Design and Validation For Task Space DOB-Based Motion Control of An Industrial Robot

Kangwagye Samuel[1], Kevin Haninger[2], Sehoon Oh[1], and Chan Lee[3]

***Abstract*— In conventional robust motion control systems, disturbance observer (DOB) nominal models are designed with same order as the actual plant such that the nominal model directly cancels with the actual plant dynamics. However, for multi-DOF systems such as 6-DOF industrial robots, identifying the higher-order model is laborious. Moreover, there is a high risk of obtaining a nominal model with large deviation from the actual plant due to severe parameter uncertainty. Thus, a reduced-order nominal model is derived from the actual plant model and compared with the one which same order as the actual plant in this paper. The designed model is simple, easy to identify and implement. From the analyses and experiment results, DOB with the proposed nominal model is not affected by severe robot model uncertainty and show significant improvement in motion control performance in terms of transient response and tracking accuracy.**

I. Introduction

Disturbance observers (DOB) [1], [2] have been shown to improve performance in motion control systems by estimating and canceling the disturbances such as friction [3], model uncertainties, unmodeled dynamics, and external uncontrolled forces [4]. Because of this, the DOBs have been utilized in motion control systems in both single degree-of-freedom (DOF) [5] and multi-DOF systems [6]–[8]. The disturbances are estimated by subtracting the command input from the result of product of the output response and the inverse of a nominal model [9], [10].

In conventional DOB-based control systems, the nominal model is designed with the same order as the actual plant model. Thus, the nominal model should be as accurate as the actual plant dynamics since severe model uncertainties make it hard to completely suppress the disturbances to achieve accurate control performance [11]. Moreover, it is difficult to guarantee closed-loop system stability if large model uncertainties exist [4]. Another important advantage of DOB-based control over other control methods is preserving the nominal performance [12]–[14]. However, guaranteeing the nominal performance recovery characteristic is difficult if the nominal model deviates largely from the actual plant due to parameter uncertainties [12].

With single-DOF systems, such as motor models, it is easy to identify the accurate nominal model since the model is simple and has few parameters. However, multi-DOF systems such as 6-DOF fixed position/velocity-controlled industrial robots have complex non-linear models which makes it difficult to identify an accurate DOB nominal model [15] or apply linear design techniques.

To this end, this paper focuses on designing simple and easy to identify nominal model for DOB with application to motion control improvement for a fixed position/velocity-controlled multi-DOF industrial robot system. The major requirement for DOB designed with the proposed nominal model is that it should be robust against severe robot model uncertainty. The contribution of this paper is summarized as

1) First, a simplified linear task space model of the target 6-DOF velocity-controlled industrial robot is derived empirically by nonparametric system identification method and validated.
2) Then, a linear DOB which estimates disturbances using the command velocity, measured velocity output, and an inverse model is designed and implemented in task space built around the position/velocity control loop.
3) Finally, a reduced-order nominal model is derived from the actual complex motion-controlled robot dynamic model and a guideline for determining its single design parameter is presented.

The rest of the paper is organized as follows. Section II describes the robot and presents the system measurement and model identification. Section III presents the improved control architecture from which the nominal model is proposed. Theoretical closed-loop analysis and verification through experiments are then conducted in Section IV. Finally, the conclusion is given in Section V.

II. Robot System Description, Measurement, and Linear Model Identification

A. Description and Task Space Modeling of the Fixed Position/Velocity-Controlled Industrial Robot

The target robot is a COMAU RACER-7-1.4 industrial manipulator shown in Fig. 1. In this paper, only linear Cartesian DOFs, i.e., joints 1/2/3 of the robot, are under consideration to provide linear motions along the x/y/z-axes. The linear motion is typically more important for performance than rotational motion. The position control interface of the robot is used, where the position commands

*This work was supported in part by the Technology Innovation Program (20015101) funded by the Ministry of Trade, Industry & Energy (MOTIE, Korea), in part by the DGIST R&D Program of the Ministry of Science and ICT (23-PCOE-02), in part by the European Union's Horizon 2020 research and innovation programme under grant agreement No 820689 — SHERLOCK, and in part by the National Research Foundation of Korea (NRF) grant funded by the Korea government (MSIT) (No.2022R1A4A3029480).

[1]Department of Robotics and Mechatronics Engineering, DGIST, Daegu, 42988, Korea [ksamuel27, sehoon]@dgist.ac.kr

[2]Department of Automation, Fraunhofer IPK, Berlin, Germany kevin.haninger@ipk.fraunhofer.de

[3]Department of Robotics Engineering, Yeungnam University, Gyeongsan, 38541, Korea chanlee@yu.ac.kr

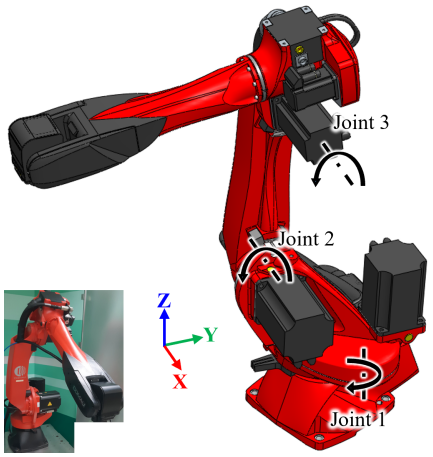

Fig. 1. Detailed 3D view of the COMAU RACER-7-1.4 robot showing the joints under consideration. Inset is the actual robot.

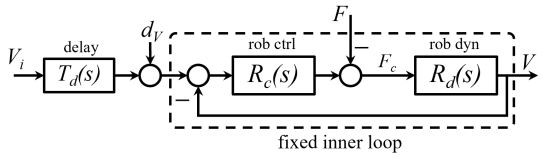

Fig. 2. Task space model for the velocity-controlled robot. V_i, V, d_V, and F are command velocity, response velocity, external disturbances, and feedback force, respectively.

can be sent in joint or Cartesian coordinates and the robot position/velocity can be measured in task space but the robot can not be directly controlled. Control is commanded in the robot's Tool Center Point (TCP), where the total control is diagonal and each DOF is independent.

A linear model will be considered to allow frequency-domain analysis, with the effect of nonlinear dynamics considered in Section IV.B. Let the velocity-controlled robot in Fig. 1 be represented by the simple block diagram in Fig. 2 for a linear single-DOF in task space [8], [16]. The velocity controller, $R_c(s)$, computes a controlled force input to the linearized robot dynamics, $R_d(s)$, where $T_d(s)$ is the time delays between the internal and external robot controllers. Note that feedback force, F, is due to e.g., payload or contact with environment. Therefore, the effect of F is ignored in this paper since only free space motion with no payload and environment contact is considered. To this end, the transfer function for the fixed inner velocity control loop can be derived for Fig. 2 as

$$R(s) = \frac{R_c(s)R_d(s)}{1 + R_c(s)R_d(s)}. \quad (1)$$

Representing the complex robot system in Fig. 1 with Fig. 2 and (1) is a big assumption considering the non-linearity and coupling issues associated with the robot, which cannot be ignored. To abate these issues, identification of the task space model $R(s)$ in (1) is conducted empirically by nonparametric system identification technique as discussed in the following subsection.

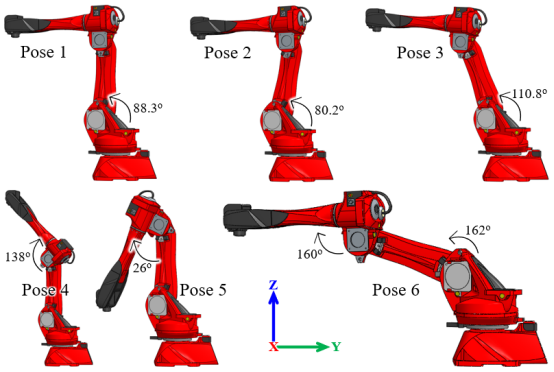

Fig. 3. Robot poses for system measurement and identification.

B. Task Space System Measurement and Model Identification

1) Task Space Robot System Measurement: Under position control, a Schroeder multisine [17, §5], [18] is utilized as an excitation signal and supplied to the position-controlled robot as the desired position. Six robot poses are considered as illustrated in Fig. 3 and for each pose, five experiments are conducted in each of the x/y/z-directions. This is done for two reasons: 1) to cover all range of robot operation space and 2) to account for uncertainty due to robot model variations which is crucial for accurate model identification.

The desired and measured position information are then differentiated using a low-pass filter (LPF) with high cutoff frequency to obtain the corresponding velocity information. The frequency response functions (FRFs) from command velocity to the measured velocity are calculated for all the robot poses and grouped in terms of axis of excitation. Their bode magnitude characteristics along with the averages are plotted in Fig. 4. It can be observed that, irrespective of the pose, the robot responds differently depending on the axis of excitation. And for each axis, similar pattern is observed, however, variations occur after the cross-over frequency which can be attributed to the effect of change in elbow joint pose. The variations occur in terms of antiresonance and resonance modes which are observed after around 13 Hz in the measured FRF. This can attributed to joint flexibility originating from the flex-splines of the harmonic drives installed in the robot in Fig. 1. Thus, it can be concluded from these results that the robot system in Fig. 1 can be considered as a flexible joint robot (FJR) system [19], [20] with motor-side and link-side dynamics with finite stiffness, i.e., flexibility, between them.

2) Task Space Linear Model Identification: To begin, the closed loop model, $R(s)$ is identified by fitting as shown by the black-dashed lines in Fig. 4(bottom) as follows.

To include the antiresonance and resonance modes exhibited after around 13 Hz in the measured FRF, the robot dynamics, $R_d(s)$, are modelled as a two-mass system illustrated in Fig. 5. The task space model in Fig. 5 is analogous to the flexible joint robot (FJR) representation in joint space [21]. Where the first and second masses, i.e., $R_{d1}(s)$ and $R_{d2}(s)$ are comparable to the joint space motor-side dynamics and

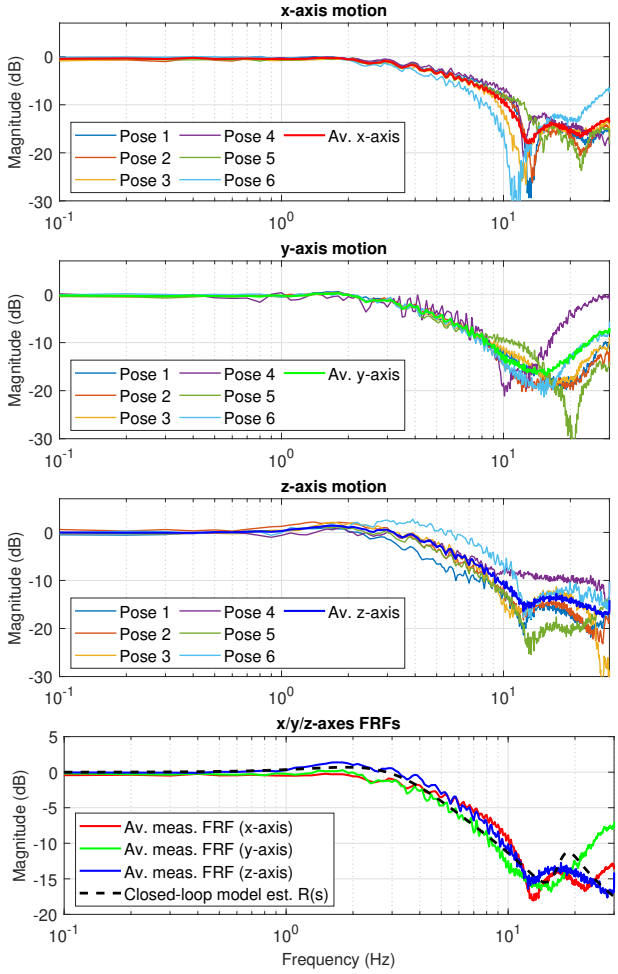

Fig. 4. Velocity-controlled robot system measurement experiment results.

link-side dynamics, and $K_s(s)$ is the stiffness dynamics that connects $R_{d1}(s)$ and $R_{d2}(s)$. These models are defined in Laplace domain as shown below

$$R_{d1,2}(s) = \frac{1}{M_{r1,2}s + B_{r1,2}} \quad \text{and} \quad K_s(s) = \frac{k_s}{s}, \tag{2}$$

where $M_\bullet$, $B_\bullet$, and k_s are mass, damping, and stiffness, respectively. Considering F_c as the input and V the output, the two-mass system in Fig. 5 can be reduced to a single transfer function describing the task space linear robot dynamics as

$$R_d(s) = \frac{\mathcal{V}}{\mathcal{F}_c}(s) = \frac{R_{d1}(s)[1 + K_s(s)R_{d2}(s)]}{1 + K_s(s)[R_{d1}(s) + R_{d2}(s)]}, \tag{3}$$

where $\mathcal{V}$ and $\mathcal{F}_c$ are the Laplace transforms of V and F_c, respectively. The equivalent task space controller, $R_c(s)$, is modelled as a proportional-integral (PI) controller as

$$R_c(s) = k_p + \frac{k_i}{s}. \tag{4}$$

Equations (3) and (4) are substituted in (1), then fit with the measured FRF as shown by the black dashed-lines in Fig. 4, from which numerical transfer functions are identified

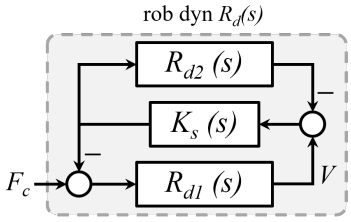

Fig. 5. Robot dynamics modelled as a two-mass system.

and given below

$$R_c(s) = 2000 + \frac{40000}{s}, \quad T_d(s) = e^{-0.003s},$$
$$R_d(s) = \frac{0.01125s^2 + 0.3656s + 112.5}{s^3 + 35s^2 + 1.258e4s + 1.063e5}, \tag{5}$$

and are used in the analyses in the Sections that follow.

III. DOB Design and Derivation of Proposed Nominal Model

A. The DOB Structure

It is a big assumption to utilize the task space linear model in Fig. 2 to represent the non-linear complex robot system. Thus, it is expected that the non-linearity and coupling effects not considered in linear model derivation are large and need to be suppressed. In addition, the external velocities, d_V, act on the robot system, causing deviation from expected motion control performance. Therefore, the DOB is designed to suppress the effects of the external velocities and eliminate the residuals of non-linearities and coupling effects.

A block diagram illustrating the DOB design and implementation is presented in Fig. 6 where the estimated lumped disturbances are given by $\hat{d}$. To make $P_n^{-1}(s)$ proper, the Q-filter is designed as a LPF, as shown below

$$Q(s) = \frac{\omega_Q}{s + \omega_Q}, \tag{6}$$

where ω_Q is the Q-filter cutoff frequency.

In conventional DOB designs, the generalized DOB nominal model, $P_n(s)$, is designed with the same order as the plant, in this case, the plant is the robot dynamics, $R_d(s)$. However, this is not possible for the case in Fig. 6 since the DOB is implemented in the outer loop as compared to the conventional inner-loop DOB implementations [22]. This is because the velocity control inner-loop of the industrial robot is closed and can not be accessed for control design improvement. Thus, in the next section, the nominal model is designed from the closed-loop plant $P(s)$.

B. Design and Limitation of the Full-Order DOB Nominal Model

From the DOB structure in Fig. 6, the nominal model, $P_n(s)$, is designed as the closed-loop dynamics of the velocity control loop, i.e., $R(s)$ in (1) as shown below

$$P_n^*(s) = R(s) = \frac{R_{cn}(s)R_{dn}^*(s)}{1 + R_{cn}(s)R_{dn}^*(s)}, \tag{7}$$

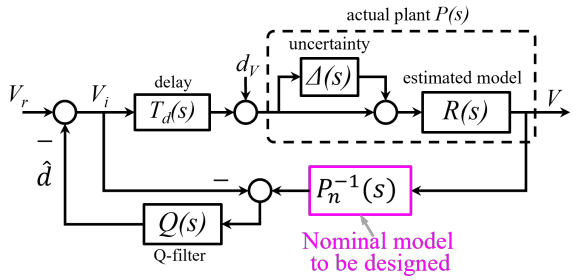

Fig. 6. DOB-based velocity control block diagram where $Q(s)$ is the Q-filter and $P_n(s)$ is the generalized DOB nominal model to be designed.

where $R_{cn}(s)$ is the nominal model of $R_c(s)$ in (4), and for simplicity of design and analysis, let $R_{cn}(s) = R_c(s)$ from now on-wards. The focus of this paper is on design of $R^*_{dn}(s)$ - the nominal model of $R_d(s)$ in (3).

The conventional way is to design $R^*_{dn}(s)$ in (7) with same order as the actual dynamics $R_d(s)$ in (3) as shown below

$$R^*_{dn}(s) = \frac{R_{d1n}(s)[1 + K_{sn}(s)R_{d2n}(s)]}{1 + K_{sn}(s)[R_{d1n}(s) + R_{d2n}(s)]}. \tag{8}$$

However, the nominal model in (7) is laborious to identify due to many parameters for (8), moreover, these increase model uncertainty. In addition, implementation of the DOB with (7) to the existing robot platform is also challenging.

C. Development of the Proposed Nominal Model

To mitigate the drawbacks of $P^*_n(s)$ in (7), the nominal model with simple and different structure from (7) is proposed as shown below

$$P^{\text{prop}}_n(s) = \frac{1}{\tau_n s + 1}. \tag{9}$$

Compared to (7) and the conventional 1-DOF single mass-based DOB models of mass-damper structure [22], the proposed model in (9) has a LPF structure with one parameter - the time constant, τ_n. This makes it more elegant, simple, and less susceptible to model uncertainty. Note that, τ_n is a task space parameter and is designed by the following criteria.

To begin with, $R^*_{dn}(s)$ in (8) can be simplified as follows. Firstly, divide through the numerator and denominator of (8) by $K_{sn}(s)$. Since k_s is relatively large, the terms with $K^{-1}_{sn}(s)$ are small and ignored. The result is further simplified to give a reduced-order version of $R^*_{dn}(s)$ given by the expressions below

$$\begin{aligned} R^{**}_{dn}(s) &= \frac{R_{d1n}(s)[K^{-1}_{sn}(s) + R_{d2n}(s)]}{K^{-1}_{sn}(s) + R_{d1n}(s) + R_{d2n}(s)} \\ &= \frac{1}{R^{-1}_{d1n}(s) + R^{-1}_{d2n}(s)} = \frac{1}{M_{rn}s + B_{rn}}, \end{aligned} \tag{10}$$

where $M_{rn} = M_{r1n} + M_{r2n}$ and $B_{rn} = B_{r1n} + B_{r2n}$. Thus, $R^{**}_{dn}(s)$ in (10) is a single-mass system as compared to the two-mass system in (8). Substituting (10) in (7) leads to a simplified nominal model given below

$$\begin{aligned} P^{**}_n(s) &= \frac{R_{cn}(s)R^{**}_{dn}(s)}{1 + R_{cn}(s)R^{**}_{dn}(s)}, \\ &= \frac{k_{pn}s + k_{in}}{M_{rn}s^2 + (k_{pn} + B_{rn})s + k_{in}}. \end{aligned} \tag{11}$$

Note that, (9) should be equivalent to (11) and (7). Utilizing this condition, re-arrange (11) and equate the result to (9) to get

$$\frac{M_{rn}s^2 + B_{rn}s}{k_{pn}s + k_{in}} = \tau_n s. \tag{12}$$

Next, considering the low frequency region by letting $s = 0$, the nominal time constant τ_n is calculated as shown below

$$\tau_n = \left| \frac{M_{rn}s + B_{rn}}{k_{pn}s + k_{in}} \right|_{s=0} = \frac{B_{rn}}{k_{in}}. \tag{13}$$

From (13), task space parameter τ_n can be calculated as the ratio of damping to integral coefficients.

To summarize, $P^{\text{prop}}_n(s)$ in (9) is a first-order transfer function, which is a reduced-order version of $P^{**}_n(s)$ in (11) and $P^*_n(s)$ in (7). Moreover, $P^{\text{prop}}_n(s)$ has a single tuning parameter, τ_n, calculated using (13). Thus, the parameter identification burden has been significantly reduced and the nominal model can be easily implemented on the existing software platform for the robot in Fig. 1. Note that, τ_n in (13) can be interpreted in terms of bandwidth as $k_{in}/(2\pi B_{rn})$ Hz to provide the initial value for easier tuning during experiments. However, in spite of its elegance and simplicity, the single tuning parameter of $P^{\text{prop}}_n(s)$ limits the freedom of design as compared to $P^{**}_n(s)$.

Note that, the nominal model in (11) is much simpler compared to (7) and can also be used for DOB design. Compared to (7), (11) has only four parameters to be identified. This reduces the model complexity, and thus the model error and parameter identification burden are also reduced. However, in comparison to $P^{\text{prop}}_n(s)$ in (9) and the conventional DOBs whose nominal models are first-order transfer functions, $P^{**}_n(s)$ in (11) is a second order transfer function with a zero in the numerator. In the next discussions, performance analysis is conducted to validate the proposed $P^{\text{prop}}_n(s)$ and comparison is made with $P^{**}_n(s)$ and $P^*_n(s)$.

D. Theoretical Validation of the Proposed Nominal Model

The numerical values of the designed nominal models are identified by fitting $P^*_n(s)$ and $P^{**}_n(s)$ with the measured FRF in Fig. 4, and are given below

$$\begin{aligned} &R_{cn}(s) = R_c(s), \;\; R^*_{dn}(s) = R_d(s), \\ &\text{and} \;\; R^{**}_{dn}(s) = \frac{1}{50s + 750}. \end{aligned} \tag{14}$$

To this end, the initial value of τ_n is calculated from the obtained values of k_{in} and B_{rn} in (14) as $\tau_n = 0.01875$.

The frequency characteristics of all the nominal models are shown by the bode magnitude plot in Fig. 7. It can be observed that all the nominal models are equivalent in the low frequency region but $P^{\text{prop}}_n(s)$ and $P^{**}_n(s)$ show different

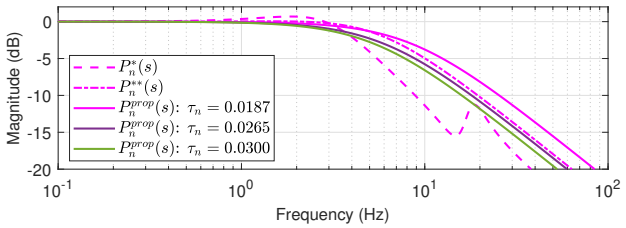

Fig. 7. Bode magnitude plots of the nominal models

behavior from $P_n^*(s)$ after their cut-off frequencies due to their structural differences. The advantage with $P_n^{\text{prop}}(s)$ and $P_n^{**}(s)$ is that the effects of joint flexibility shown by $P_n^*(s)$ can be eliminated since the anti-resonance and resonance modes are inside their bandwidths. Moreover, $P_n^{**}(s)$ and $P_n^{\text{prop}}(s)$ exhibit higher bandwidth than $P_n^{**}(s)$. However, $P_n^{\text{prop}}(s)$ exhibits less steeper slope in high frequency region than $P_n^{**}(s)$. Note that, as mentioned earlier, $\tau_n = 0.0163$ in (14) can be interpreted in terms of bandwidth as $1/(2\pi \times 0.0163) = 9.7641$ Hz, which is the cutoff frequency for $P_n^{\text{prop}}(s)$ in Fig. 7. Thus, 0.0163 can be considered as the minimum value of τ_n, moreover, τ_n can be increased to 0.0300 maximum, i.e., at 5.3 Hz cutoff frequency as shown in Fig. 7 (green color). In conclusion, $0.0163 \leq \tau_n \leq 0.0300$ is the margin or range of values that τ_n can be designed to keep the resonance and antiresonance modes within the bandwidth of $P_n^{\text{prop}}(s)$.

IV. Theoretical Closed-Loop Analysis And Experimental Verification

A. Time Response Analysis

A step response of (16) is utilized to analyze the behavior of the proposed nominal model in terms of transient response and steady state behaviors. Moreover, to examine the effect of variation in Q-filter cutoff frequency, step responses when $\omega_Q = 1, 5, 15, 30$ Hz are computed and plotted in Fig. 8. The numerical values in (5) and (14) are utilized.

Most importantly, it can be observed for all the ω_Q values that, DOB with $P_n^{\text{prop}}(s)$ and $P_n^{**}(s)$ improves the steady-state tracking performance as compared to the DOB with conventional nominal model design, $P_n^*(s)$, and No DOB cases. Also, increasing ω_Q reduces the settling time and peak velocity for DOB with $P_n^{\text{prop}}(s)$ and $P_n^{**}(s)$ but has no influence for DOB with $P_n^{**}(s)$ case. Moreover, it can be confirmed in the bottom row that τ_n for $P_n^{\text{prop}}(s)$ can be further increased to significantly improve the steady-state response and tracking accuracy.

To quantitatively validate the proposed nominal model, the transient response and tracking performance characteristics are computed for Fig. 8 when $\omega_Q = 15$ Hz and $\tau_n = 0.0265$. These are presented in Table I. Apart from the % overshoot characteristic where the DOB with $P_n^{\text{prop}}(s)$ exhibits the best performance with the least value (5.9207), other characteristics are comparable to those of DOB with $P_n^{**}(s)$. This result validates the utilization of the reduced-order nominal model, $P_n^{\text{prop}}(s)$, proposed in (9).

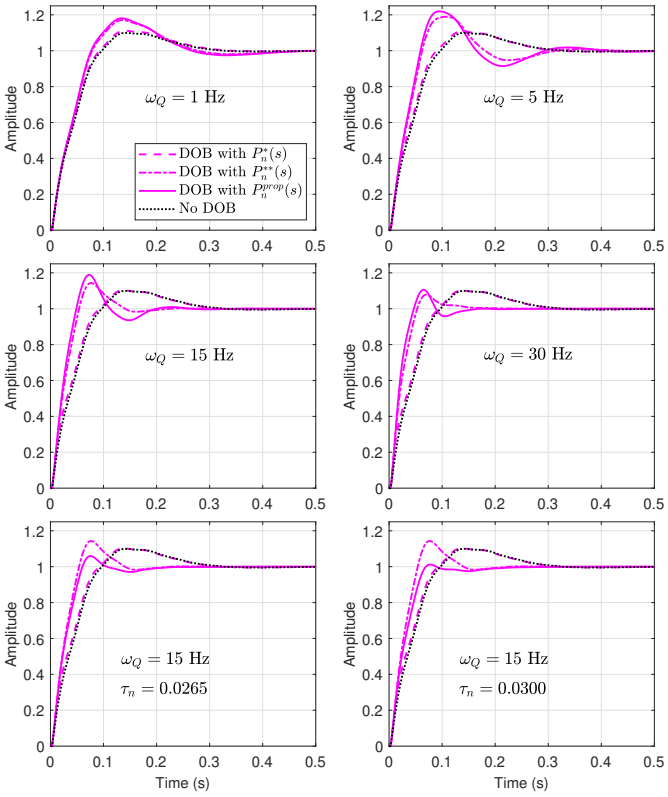

Fig. 8. Step response theoretical results where $\tau_n = 0.0187$ in the first and second rows.

TABLE I
Quantitative Step Response Characteristics For Fig. 8

Characteristic	**Values for $\omega_Q = 15$ Hz and $\tau_n = 0.0265$**			
	No DOB	DOB with		
		$P_n^*(s)$	$P_n^{**}(s)$	$P_n^{\text{prop}}(s)$
Rise time	0.0665	0.0632	0.0397	0.0438
Settling time	0.2712	0.2676	0.1298	0.1714
% overshoot	9.9353	10.2970	14.3198	5.9207
Peak	1.0994	1.1030	1.1432	1.0592
Peak time	0.1417	0.1369	0.0764	0.0761

B. Behavior of Proposed Nominal Model Against Severe Robot Model Uncertainty

In this paper, linear models are used on the non-linear robot system, however, the effective linearized dynamics change depending on robot pose. Where large model deviation is especially caused by the pose of elbow joint. Performance of the designed DOB utilizing the proposed nominal model in (9) should not be affected by variation in model uncertainty.

Thus, robustness of proposed DOB nominal model against robot model uncertainty is checked for different robot poses, where pose 2 and pose 4 (see Fig. 3) are considered in this paper. And the small gain theorem [23], [24] is utilized to verify robustness against uncertainty. The small gain theorem condition for the input multiplicative variation in the robot

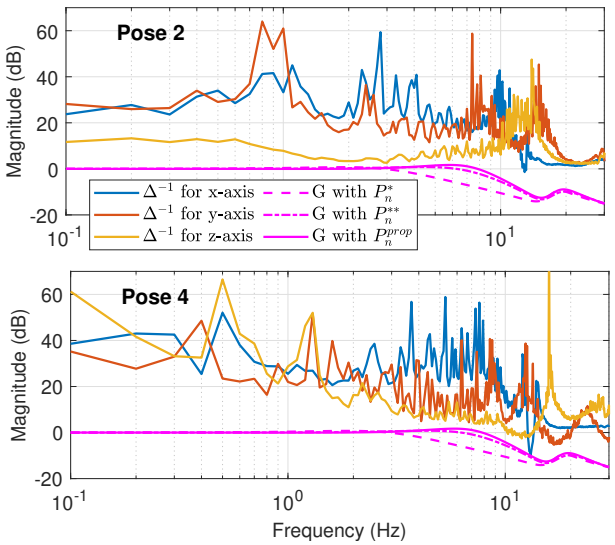

Fig. 9. Result for stability against severe model uncertainty when $\omega_Q = 15$ Hz and $\tau_n = 0.0187$, showing that (15) holds.

model is derived for Fig. 6 as

$$\|G(j\omega)\| < \left\|\Delta^{-1}(j\omega)\right\|, \tag{15}$$

where $\Delta(j\omega)$ is the model uncertainty and $G(j\omega)$ is the complimentary sensitivity function, which is same as the transfer function from V_r to V given below

$$G(j\omega) = \frac{T_d(j\omega)R(j\omega)}{1 - Q(j\omega) + T_d(j\omega)R(j\omega)Q(j\omega)P_n^{-1}(j\omega)}, \tag{16}$$

where $R(j\omega)$ is the identified model given in (1). Given that $P(j\omega)$ is the actual plant (see Fig. 6), given as

$$P(j\omega) = [1 + \Delta(j\omega)]R(j\omega), \tag{17}$$

the inverse input multiplicative uncertainty is calculated as

$$\Delta^{-1}(j\omega) = \frac{R(j\omega)}{P(j\omega) - R(j\omega)}, \tag{18}$$

Equation (18) is used to calculate inverse of the model uncertainty from the data measured in Section II-B.1. Robot poses 2 & 4 (see Fig. 3) are considered, and for each pose the inverse uncertainty in x/y/z directions are calculated. The bode magnitudes of (18) and (16) - using the nominal models in (7), (9), and (11) are plotted in Fig. 9 when $\omega_Q = 15$ Hz and $\tau_n = 0.0187$. It is validated from the results in Fig. 9 that, the control method with the proposed nominal model is robust against severe robot model variations despite being of simple structure and linear on a non-linear robot system.

C. Motion Control Experimental Validation

To verify the effectiveness of the proposed DOB nominal model, motion control experiments are conducted on the COMAU RACER-7-1.4 robot in Fig. 1 as follows.

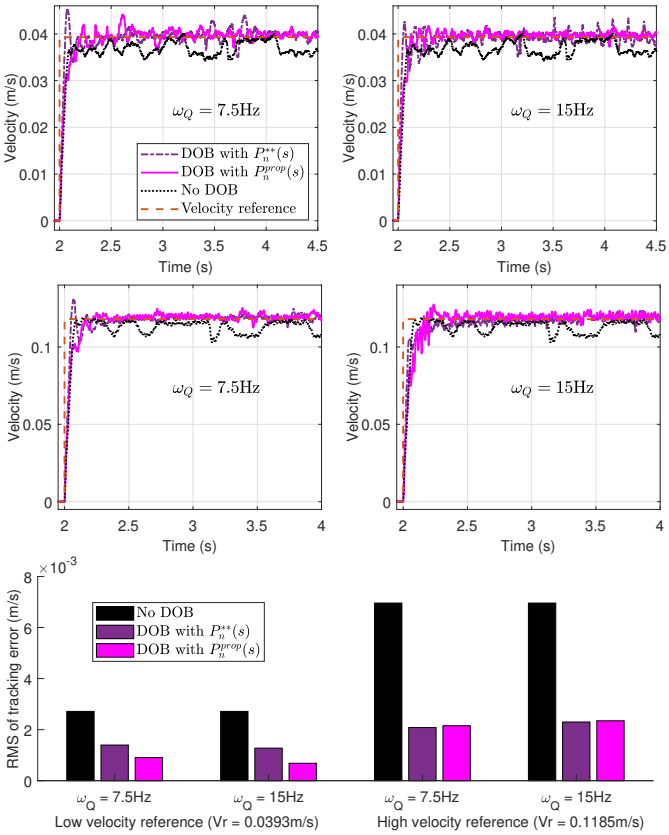

Fig. 10. Step response experiment results. $\tau_n = 3.18$ and, top row: slow motion ($V_r = 0.0393$ m/s), middle row: fast motion ($V_r = 0.1185$ m/s), and bottom row: RMS values of velocity tracking errors

1) Experiment Protocol: The nominal parameters of $P_n^{**}(s)$ in (11) are empirically tuned as $k_{pn} = 100$, $k_{in} = 400$, $M_{rn} = 2.5$, and $B_{rn} = 20$. These are utilized through out all the experiments that follow. With the robot in Pose 1 (see Fig. 3), a step signal is supplied as the reference velocity, V_r, in the x-axis direction at 2 s. Experiments are conducted for DOB with $P_n^{**}(s)$, DOB with $P_n^{\text{prop}}(s)$, and No DOB methods, and the results are compared. DOB with $P_n^{*}(s)$ method is not considered since it is difficult to tune the many parameters of $R_{dn}^{*}(s)$ in (8). Motion control performance is evaluated in terms of transient response and reduced velocity tracking error in steady-state.

2) Experiment Results: Fig. 10 presents the step experiment results where first row is for slow motion, middle row is for fast motion, and the bottom row shows the bar graph of root mean square (RMS) values of the velocity tracking errors for all the methods and motion speeds.

For the slow motion case, it can be observed that the proposed method, i.e., DOB with $P_n^{\text{prop}}(s)$ exhibits the best steady-state tracking performance with least RMS values as compared to DOB with $P_n^{**}(s)$ method. Whereas both methods show comparable tracking performance for the fast motion case. An increase in Q-filter cut-off frequency improves the tracking performance for both methods.

However, in the transient region, the DOB with $P_n^{**}(s)$ model has a larger overshoot in all the speeds as compared

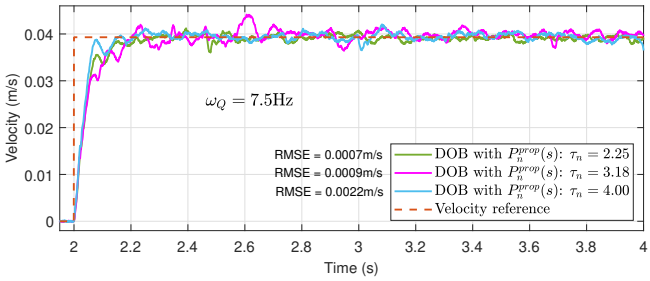

Fig. 11. Experiment result for only DOB with $P_n^{\text{prop}}(s)$ method when τ_n is varying. $\omega_Q = 7.5$ Hz and $V_r = 0.0393$ m/s.

to the proposed method, which has no overshoot. This result matches the theoretical results in Fig. 8 of Section IV-A.

On the other hand, the No DOB method exhibits a transient response with less overshoot and good rise time, however, there is significant deterioration in tracking performance due to its inability to suppress the effects of disturbances such as nonlinear friction and gear cogging. This is confirmed by the very large tracking errors in both speeds as shown by the bar graph in Fig. 10.

Further, the slow motion experiment is repeated only for the DOB with $P_n^{\text{prop}}(s)$ method at various τ_n values and the results are presented in Fig. 11. The transient response does not show a significant difference for all the values of τ_n. For tracking performance in steady-state, it is observed that reducing the time constant improves the tracking performance. This performance is confirmed by the calculated RMSE values as indicated in the figure legend for each value of τ_n where $\tau_n = 2.25$ results in the least RMSE value, i.e., 0.0007 m/s.

V. Conclusions

In this paper, model reduction techniques have been employed to design simple DOB models which have few parameters to identify and easy to implement on the robot software platform. Analysis and experiments show that DOB with the proposed nominal model is robust against model uncertainty, is able to suppress disturbances and preserve nominal performance, thus significantly improving velocity control performance in terms of transient response and steady-state accuracy.

References

[1] K. Ohnishi, M. Shibata, and T. Murakami, "Motion control for advanced mechatronics," *IEEE/ASME transactions on mechatronics*, vol. 1, no. 1, pp. 56–67, 1996.

[2] S. Oh and K. Kong, "High-precision robust force control of a series elastic actuator," *IEEE/ASME Transactions on mechatronics*, vol. 22, no. 1, pp. 71–80, 2016.

[3] K. Samuel, R. Oboe, and S. Oh, "Twofold observer-based precise force control," *IEEE Transactions on Control Systems Technology*, vol. 30, no. 5, pp. 2251–2260, 2022.

[4] S. Li, J. Yang, W.-H. Chen, and X. Chen, *Disturbance observer-based control: methods and applications*. CRC press, 2014.

[5] K. Samuel, K. Haninger, R. Oboe, and S. Oh, "Integrated disturbance observer-based robust force control," *IEEE Transactions on Industrial Electronics*, pp. 1–11, 2022, doi: 10.1109/TIE.2022.3224189.

[6] S. Komada, N. Machii, and T. Hori, "Control of redundant manipulators considering order of disturbance observer," *IEEE Transactions on Industrial Electronics*, vol. 47, no. 2, pp. 413–420, 2000.

[7] Z. Li, C.-Y. Su, L. Wang, Z. Chen, and T. Chai, "Nonlinear disturbance observer-based control design for a robotic exoskeleton incorporating fuzzy approximation," *IEEE Transactions on Industrial Electronics*, vol. 62, no. 9, pp. 5763–5775, 2015.

[8] K. Samuel, K. Haninger, and S. Oh, "High-performance admittance control of an industrial robot via disturbance observer," in *IECON 2022–48th Annual Conference of the IEEE Industrial Electronics Society*, pp. 1–6, IEEE, 2022.

[9] E. Sariyildiz, H. Sekiguchi, T. Nozaki, B. Ugurlu, and K. Ohnishi, "A stability analysis for the acceleration-based robust position control of robot manipulators via disturbance observer," *IEEE/ASME Transactions on Mechatronics*, vol. 23, no. 5, pp. 2369–2378, 2018.

[10] K. Samuel, J. Kim, and S. Oh, "Performance comparison of position controlled robotic stage when force-and position-based disturbance observers are implemented," in *2021 21st International Conference on Control, Automation and Systems (ICCAS)*, pp. 994–999, IEEE, 2021.

[11] J. Back and H. Shim, "Adding robustness to nominal output-feedback controllers for uncertain nonlinear systems: A nonlinear version of disturbance observer," *Automatica*, vol. 44, no. 10, pp. 2528–2537, 2008.

[12] G. Park, Y. Joo, and H. Shim, "Asymptotic rejection of sinusoidal disturbances with recovered nominal transient performance for uncertain linear systems," in *53rd IEEE Conference on Decision and Control*, pp. 4404–4409, IEEE, 2014.

[13] J. Back and H. Shim, "An inner-loop controller guaranteeing robust transient performance for uncertain mimo nonlinear systems," *IEEE Transactions on Automatic Control*, vol. 54, no. 7, pp. 1601–1607, 2009.

[14] L. B. Freidovich and H. K. Khalil, "Performance recovery of feedback-linearization-based designs," *IEEE Transactions on automatic control*, vol. 53, no. 10, pp. 2324–2334, 2008.

[15] S. Oh and K. Kong, "Two-degree-of-freedom control of a two-link manipulator in the rotating coordinate system," *IEEE Transactions on Industrial Electronics*, vol. 62, no. 9, pp. 5598–5607, 2015.

[16] K. Haninger, M. Radke, A. Vick, and J. Kruger, "Towards High-Payload Admittance Control for Manual Guidance with Environmental Contact," *IEEE Robotics and Automation Letters*, 2022.

[17] R. Pintelon and J. Schoukens, *System identification: a frequency domain approach*. John Wiley & Sons, 2012.

[18] M. Schroeder, "Synthesis of low-peak-factor signals and binary sequences with low autocorrelation (corresp.)," *IEEE transactions on Information Theory*, vol. 16, no. 1, pp. 85–89, 1970.

[19] M. J. Kim and W. K. Chung, "Robust control of flexible joint robots based on motor-side dynamics reshaping using disturbance observer (dob)," in *2014 IEEE/RSJ International Conference on Intelligent Robots and Systems*, pp. 2381–2388, IEEE, 2014.

[20] A. De Luca and W. J. Book, "Robots with flexible elements," in *Springer Handbook of Robotics*, pp. 243–282, Springer, 2016.

[21] M. J. Kim and W. K. Chung, "Disturbance-observer-based pd control of flexible joint robots for asymptotic convergence," *IEEE Transactions on Robotics*, vol. 31, no. 6, pp. 1508–1516, 2015.

[22] W.-H. Chen, J. Yang, L. Guo, and S. Li, "Disturbance-observer-based control and related methods—an overview," *IEEE Transactions on industrial electronics*, vol. 63, no. 2, pp. 1083–1095, 2015.

[23] I. D. Landau, R. Lozano, M. M'Saad, and A. Karimi, *Adaptive control: algorithms, analysis and applications*. Springer Science & Business Media, 2011.

[24] K. J. Åström and R. M. Murray, *Feedback systems: an introduction for scientists and engineers*. Princeton university press, 2021.